OXFORD

Cerebral Cortex, 2022, **00**, 1–18
https://doi.org/10.1093/cercor/bhab467
Original Article

Corticofugal Modulation of Temporal and Rate Representations in the Inferior Colliculus of the Awake Marmoset

Xiaohui Wang, Yuanqing Zhang, Siyi Bai, Runze Qi, Hao Sun, Rui Li, Lin Zhu, Xinyuan Cao, Guoqiang Jia, Xinjian Li and Lixia Gao

Department of Neurology of the Second Affiliated Hospital, Interdisciplinary Institute of Neuroscience and Technology, College of Biomedical Engineering and Instrument Science, School of Medicine, Zhejiang University, Hangzhou 310000, China
Address correspondence to Lixia Gao, Department of Neurology of the Second Affiliated Hospital, Interdisciplinary Institute of Neuroscience and Technology, College of Biomedical Engineering and Instrument Science, School of Medicine, Zhejiang University, Hangzhou 310000, China. Email: lxgao10@zju.edu.cn.

Abstract

Temporal processing is crucial for auditory perception and cognition, especially for communication sounds. Previous studies have shown that the auditory cortex and the thalamus use temporal and rate representations to encode slowly and rapidly changing time-varying sounds. However, how the primate inferior colliculus (IC) encodes time-varying sounds at the millisecond scale remains unclear. In this study, we investigated the temporal processing by IC neurons in awake marmosets to Gaussian click trains with varying interclick intervals (2–100 ms). Strikingly, we found that 28% of IC neurons exhibited rate representation with nonsynchronized responses, which is in sharp contrast to the current view that the IC only uses a temporal representation to encode time-varying signals. Moreover, IC neurons with rate representation exhibited response properties distinct from those with temporal representation. We further demonstrated that reversible inactivation of the primary auditory cortex modulated 17% of the stimulus-synchronized responses and 21% of the nonsynchronized responses of IC neurons, revealing that cortico-colliculus projections play a role, but not a crucial one, in temporal processing in the IC. This study has significantly advanced our understanding of temporal processing in the IC of awake animals and provides new insights into temporal processing from the midbrain to the cortex.

Keywords: cortical inactivation, inferior colliculus, rate representation, temporal representation, time-varying signal

Introduction

Temporal processing is crucial for sound perception and cognition (Joris et al. 2004; Mauk and Buonomano 2004; Wang et al. 2008a, 2008b; Moon and Hong 2014; Mioni et al. 2020), especially for communication sounds, such as human speech and music (Rosen 1992; Singh and Theunissen 2003; Karklin et al. 2012; Li et al. 2012; Moore 2012; Wang 2013; Theunissen and Elie 2014; Ding et al. 2017). Many natural and human-generated sounds are composed of a string of repeated acoustic events at specific repetition rates ranging from several to hundreds of Hertz, such as cricket song, heartbeat, and rhythmic structures in music (Rosen 1992; Singh and Theunissen 2003; Joris et al. 2004; Bendor and Wang 2007; Petkov and Bendor 2016). Humans perceive these sounds as continuous if the repetition rate is higher than the flutter range (10–45 Hz) or discrete if the repetition rate is below it (Bendor and Wang 2007; Nourski and Brugge 2011; Petkov and Bendor 2016). Several studies have shown that different perceptions of the repetition rate in communication and other biologically meaningful sounds largely depend on how the brain encodes their temporal structure (Joris et al. 2004; Bendor and Wang 2007; Wang et al. 2008a, 2008b; Nourski and Brugge 2011; Petkov and Bendor 2016). In awake marmosets, accumulating evidence from studies have shown that the auditory cortex (AC) uses stimulus-synchronized responses (temporal representation) to encode slowly changing time-varying stimuli and firing rate-based nonsynchronized responses to encode rapidly changing time-varying stimuli (Lu et al. 2001a, 2001b; Bendor and Wang 2007; Gao et al. 2016), which provides a reasonable interpretation of the different perceptions of sound repetition rates at the cortical level. However, the neural mechanisms underlying the temporal processing of time-varying stimuli in earlier subcortical nuclei remain unclear.

Rate representation, which is specifically defined as when a neuron uses nonsynchronized responses to encode rapidly changing time-varying stimuli, was first reported in the AC of awake marmosets (Lu et al. 2001a, 2001b) and later confirmed in awake cats (Dong et al. 2011) and rats (Gao and Wehr 2015), as well as in the medial geniculate body (MGB) of awake marmosets (Bartlett and Wang 2007). The sensory cortex is thought

Received: June 21, 2021. **Revised:** October 12, 2021. **Accepted:** November 16, 2021

to use an opponent rate-coding strategy to encode time-varying signals, in which some neurons increase their firing rate with an increasing click rate (positive-monotonic) while another set of cortical neurons change their firing rate in the opposite direction (negative monotonic). They may use a complementary code to encode time-varying signals (Petkov and Bendor 2016). Since opponent rate-coding has only been reported in the AC (Bendor and Wang 2007; Gao et al. 2016) and the somatosensory cortex of awake monkeys (Salinas et al. 2000; Romo and Salinas 2003), it is thought to only function in the cortex of the awake brain (Petkov and Bendor 2016). In contrast to the AC, neurons in the subcortical nuclei mainly use stimulus-synchronized temporal responses to encode the temporal information of sounds (Joris et al. 2004), such as the auditory nerve (Versteegh et al. 2011; Heil and Peterson 2017), cochlear nucleus (Frisina et al. 1990; Joris et al. 1994; Joris et al. 2004), and IC (Rees and Moller 1983, 1987; Langner and Schreiner 1988; Batra et al. 1989; Muller-Preuss et al. 1994; Krishna and Semple 2000; Eguia et al. 2010), as well as the MGB (Vernier and Galambos 1957; Creutzfeldt et al. 1980; Rouiller and de Ribaupierre 1982; Preuss and Muller-Preuss 1990; Bartlett and Wang 2007). However, stimulus-synchronized temporal representation deteriorates gradually along the ascending auditory pathway (de Ribaupierre et al. 1980), demonstrating decreased stimulus-following rates and reduced proportions of neurons with temporal responses (Joris et al. 2004; Bartlett and Wang 2007; Eguia et al. 2010). Taken together, given these results, it is crucial to know how the midbrain processes fast-click trains that are too fast to be encoded by stimulus-synchronized temporal responses.

The IC is the major auditory processing center in the midbrain; it receives converging inputs from all auditory brainstem nuclei and serves as a relay to the AC *via* the MGB (Aitkin et al. 1994; Suta et al. 2008; Gruters and Groh 2012; Gao et al. 2015). IC neurons have been reported to mainly use stimulus-synchronized temporal responses to encode the temporal structure of sounds (Rees and Moller 1983, 1987; Batra et al. 1989; Eguia et al. 2010). Although IC neurons can phase-lock to modulation frequencies up to 1200 Hz (Schuller 1979; Rose and Capranica 1985; Epping and Eggermont 1986; Langner and Schreiner 1988), most have a best modulation frequency below 200 Hz (Rees and Moller 1983, 1987; Batra et al. 1989; Eguia et al. 2010). The best modulation frequency is a distinct feature of IC neurons as a band-pass filter for temporal processing (Langner 1983; Muller-Preuss et al. 1994; Joris et al. 2004). However, to date, rate representation with nonsynchronized responses has never been reported in the IC, in sharp contrast to the MGB in which approximately 40% of neurons show such responses (Bartlett and Wang 2007; Wang et al. 2008a, 2008b). Thus, it is necessary to examine temporal processing in the IC of the same species in the awake state. In addition, cortical feedback projections are extensive and have been found to modulate many aspects of sound processing by IC neurons (Bajo and King 2012), such as frequency (Ma and Suga 2001a, 2001b; Zhou and Jen 2007; Blackwell et al. 2020), intensity (Yan and Ehret 2002), duration (Ma and Suga 2001a, 2001b), and spatial location (Zhou and Jen 2005; Bajo et al. 2010). We wondered whether the cortical feedback projection affects the temporal processing of IC neurons. Therefore, we designed this study to investigate the neural coding of time-varying stimuli in the IC of awake marmosets, focusing on stimulus-synchronized and firing rate-based encoding of time-varying signals, and the role of descending auditory projections in temporal processing in the IC.

Materials and Methods

All experimental procedures were approved by the Animal Use and Care Committee of Zhejiang University and followed the National Institutes of Health (USA) guidelines.

Animal Preparation

Experiments were conducted on two female adult common marmosets (*Callithrix jacchus*) using the chronic awake preparation (Lu et al. 2001a, 2001b), as described in our previous study (Gao and Wang 2020). In brief, the animals were trained to sit quietly in a customized primate chair over a course of approximately 2 weeks. Head-cap implantation surgery was performed under aseptic conditions, during which two posts were attached to the skull to fix the head for electrophysiological recordings. Two recording chambers were attached with dental cement over the temporal lobe, and the lateral sulcus was traced as a landmark to locate the AC. To access the primary auditory cortex (A1) and the IC, small craniotomies (~1 mm in diameter) were made in the recording chamber to allow the penetration of electrodes. A1 was identified by its tonotopic map along the lateral sulcus at an angle of 60° (Bendor and Wang 2008). The method of accessing the IC was the same as in previous studies (Nelson et al. 2009; Nelson and Young 2010). In brief, the recording electrode approached the IC along a dorsolateral-to-ventromedial trajectory, entering the brain in an approximately frontal plane at an angle of 45° lateral to medial. The electrode traversed 8–10 mm of brain tissue before reaching the IC. In general, 10–25 electrode penetrations were made through each mini-craniotomy, which was then sealed with dental cement, and another opened for new electrode penetrations (Gao and Wang 2020).

Acoustic Stimuli

All recording sessions were carried out in a double-walled, soundproof chamber (FOSHANHENQI, Guangzhou, China). Acoustic signals were generated digitally at a sampling rate of 97.7 kHz using the custom MatLab software (MathWorks), low-pass filtered at 48.8 kHz, converted to analog signals (RX6; Tucker-Davis

Technologies, Alachua, FL), power-amplified (PM5005, Marantz), attenuated with two serially-linked attenuators (PA5, Tucker-Davis Technologies), and delivered in free-field through a speaker (8351A, Genelec) located approximately 1.2 m in front of the animal's head. Once a neuron was encountered, its frequency-tuning profile was determined by playing pure tones 200 ms in duration with 5 ms cosine ramps that spanned 3–6 octaves around a manually determined center frequency in 0.1 octave steps. The best frequency (BF) was defined as the tone frequency that generated the highest firing rate in the recorded neuron at a sound level 20 dB above threshold. The rate-level function of the recorded neuron was determined by varying the sound intensity from −10 to 70 dB in 10-dB steps. The best level (BL) of a neuron was defined as the sound level that elicited the maximal firing rate at the BF. After the BF and BL of a neuron were determined, temporally modulated sounds (Gaussian clicks) were played in randomized blocks of five repetitions. The interclick interval (ICI) of the Gaussian clicks ranged from 2 to 100 ms (repetition rate between 10 and 500 Hz). The bandwidths of the Gaussian clicks were controlled by the SD parameter, σ, and ranged from 0.1 to 0.3. A larger σ value gave a wider temporal envelope and a narrower spectral peak. Usually, the value of σ was set to 0.2. The duration of the Gaussian click train was 500 ms.

Cryoloop Implantation and Reversible Inactivation of A1

The cooling method for awake marmosets was adopted from that developed for the AC of awake behaving cats (Lomber et al. 2010, 2011), see (Lomber et al. 1999). The animals were surgically implanted with a stainless-steel cryoloop on the surface of A1 after mapping its tonotopic organization. The cryoloop was manufactured from 17-gauge hypodermic stainless-steel tubing (1.4 mm O.D. × 1.1 mm I.D.), which was shaped into a loop that conformed to the surface of each marmoset's A1. The cooling effect was assessed by single-unit recordings in A1 (Fig. 7C) after the cryoloop was positioned in A1 using a stereotaxic micromanipulator (SM11, Narishige, Tokyo, Japan). The cryoloop assembly was secured in a dental acrylic layer in the recording chamber by dental cement (Unifast, Trad, GC Corp., Tokyo, Japan) after filling the craniotomy with silastic (KWIK-SIL, World Precision Instruments, LLC, Sarasota, FL).

Inactivation Procedure

During each experimental session, A1 was cooled by pumping chilled ethanol (histological grade) through the tubing loop (Fig. 7A). A microthermocouple (TC) was made by twisting a Teflon-insulated copper (38 AWG, 0.102 mm) and constantan wire (Omega Engineering Ltd) and attached to the cryoloop to monitor the change of temperature on the cortical surface in real time. The TC had both high resolution and a fast response time in the operating range 0–40 °C. Loop temperature was monitored and accurately regulated by controlling the rate of ethanol flow. A stable loop temperature (~3 °C) was reached within 3–5 min of initiating cooling, and normal brain temperature was regained within approximately 2 min after the cessation of cooling, consistent with previous studies (Lomber et al. 1999). A loop temperature of approximately 3 °C reliably deactivates neural activity in the AC and induces behavioral deficits (Lomber et al. 2010, 2011). During experimental sessions, inactivation of A1 lasted 5–10 min for neurophysiological recordings. Data were collected during a control block first (Before) then followed by an inactivation block (Cryo-inactivation) and a recovery block (After).

Single-Unit Recording

Single-unit recordings were made using high-impedance tungsten microelectrodes (2–5 MΩ, FHC, Inc., Bowdoin, ME) advanced by a one-axis motorized stereotaxic micromanipulator (DMA1510, Narishige). The signals were amplified (AlphaLab SNR, Alpha Omega Engineering, Nof HaGalil, Israel) and digitized (RX6, Tucker-Davis Technologies), then analyzed and saved using custom programs written in MatLab (Mathworks). Spikes were detected online using a template matching method (AlphaLab SNR, Alpha Omega Engineering).

Electrolytic Lesion and Histology

At the cessation of the electrophysiological recordings, small electrolytic lesions were made in physiologically identified regions by passing 30 μA current through the recording electrode for 60–150 s (A365 stimulus isolator, World Precision Instruments Inc). Animals were euthanized by administering an overdose of sodium pentobarbitone (100 mg/kg) and perfused transcranially with 0.9% saline, followed by 4% paraformaldehyde in 0.1 M phosphate buffer (pH 7.4). After perfusion, the brain was removed, put in a 30% sucrose solution, and frozen. Sections (30 μm) were cut on a freezing microtome through the entire extent of the IC and processed using the Nissl staining method. IC subdivisions were assigned based on parcellation schemes established in the previous studies (Newman et al. 2009; Hardman and Ashwell 2012). The locations of recorded neurons were reconstructed based on the coordinates of the tracks relative to that in which lesions were made and the depths at which the recordings occurred.

Data Analysis

Data were analyzed using custom software written in MatLab. The analysis methods used were the same as in our previous publications (Lu et al. 2001a, 2001b; Bendor and Wang 2008; Gao et al. 2016; Gao and Wang 2019). In brief, the firing rate elicited by sound was calculated over the entire stimulus duration, and the mean spontaneous rate (estimated over the entire stimulus set) was subtracted in all analyses. BF was defined as the tone frequency that generated the highest firing rate. A

rate-level function curve was generated at the BF from −10 to 70 dB in 10-dB steps. The monotonicity index (MI) was defined as the ratio of the mean firing rate at the highest sound level tested (70 dB SPL) to the mean firing rate at the BL of the neuron. Neurons with an MI > 0.75 were defined as having a monotonic rate level function whereas neurons with MI ≤ 0.75 were defined as having a nonmonotonic rate level function (Bendor and Wang 2008). The half bandwidth was defined as the tuning bandwidth at which the firing rate was ≤50% of the peak firing rate on both sides of the peak. The time after stimulus onset at which the spike count in a bin of the cumulative peristimulus time histogram exceeded twice the largest SD of the spontaneous firing rate was calculated as the minimum response latency. The bin-width used in this calculation was 1 ms. The response threshold was defined as the minimum sound level that evoked a response that was significantly different from the spontaneous firing rate.

The stimulus-synchronized spiking response was quantified by the vector strength (VS), which was computed from the following formula (Goldberg and Brown 1969; Lu et al. 2001a, 2001b):

$$VS = \frac{1}{n}\sqrt{\left(\sum_{1}^{n}\cos\theta i\right)^2 + \left(\sum_{1}^{n}\sin\theta i\right)^2}$$

$\theta i = 2\pi\frac{ti}{T}$, where n is the number of spikes evoked by an acoustic stimulation 50 ms after stimulus onset to the end of the stimulus; ti is the time of spike occurrence, and T is the ICI. VS provides a quantitative analysis of stimulus-synchronized spiking response, which may vary from 0 to 1. A value of 1 implies perfect synchrony between acoustic stimulation and the auditory response. A value of 0 implies a random relation between them. Significance of the stimulus-synchronized spiking response was statistically assessed with Rayleigh statistics (RS, $2n^{*}VS^2$) (Goldberg and Brown 1969; Lu et al. 2001a, 2001b), the values of which >13.8 was equivalent to $P < 0.001$. The RS was computed for the first half and the second half of the stimulus and the minimum value was used. This excluded some responses that were synchronized during only a part of the stimulus. For each unit, the minimum ICI at which the neuron significantly synchronized with the stimulus was defined as the synchronization boundary. This was the lower boundary at which there was significant synchronization to the click train. For responses not synchronized to the stimulus (Rayleigh statistic values ≤13.8), Spearman's correlation coefficient was used to assess the correlation between the neural firing rate and the repetition rate of Gaussian click trains. Positive-monotonic nonsynchronized responses were identified if the Spearman correlation coefficient was ≥0.4, and negative-monotonic nonsynchronized responses were identified if the Spearman correlation coefficient was ≤−0.4. A discharge rate ratio was used to further quantify the nonsynchronized response (Lu et al. 2001a, 2001b), which is defined as the maximum discharge rate occurring at ICIs ≤5 ms divided by the maximum discharge rate occurring at ICIs > 30 ms.

All values are expressed as the mean ± SEM unless otherwise specified. Data in the results were analyzed with ANOVA and those obtained before and after inactivation of A1 were analyzed with paired t-test. P values < 0.05 were considered statistically significant for all analyses and were indicated with asterisks, such as $^{*}P$ values < 0.05, $^{**}P$ values < 0.01, $^{***}P$ values < 0.001, and $^{****}P$ values < 0.0001.

Results

Identification of IC Neurons Based on Electrophysiological Properties

While the posts attached to the top of the skull fixed the head, the IC was accessed from the laterally placed recording chamber (Fig. 1A). Based on the atlas of the marmoset brain, the IC is located ventral and posterior to A1 (Fig. 1B). To successfully record neural activity in the IC, an electrode penetrated the dura at 45° relative to the horizontal plane through a 1 mm craniotomy posterior to the AC (Fig. 1A–D), as in previously published methods (Nelson et al. 2009; Nelson and Young 2010). When the electrode was advanced in a dorsolateral-to-ventromedial trajectory, atypical auditory responses with broad tuning were detected first (Fig. 2A,C), and then neurons with sharp frequency-tuning were recorded (Fig. 2B,D). A remarkable feature of the IC is its well-defined tonotopic organization (Aitkin et al. 1994). To confirm that we were recording in the IC, we measured the BF, response latency, and tuning bandwidth of all the neurons recorded in each penetration (Fig. 2E–G). We found that the BF of these neurons increased (Fig. 2E), and the tuning bandwidth decreased (Fig. 2G) with depth in a recording track. We reconstructed a tonotopic map of the IC based on the location of the electrode penetration and the recording depth of each neuron (Fig. 2H,I), which demonstrated a well-organized tonotopic map and confirmed that the neurons were recorded from the IC.

Previous studies have reported that the marmoset IC has three subdivisions (Fig. 1E): the central nucleus (CIC), dorsal cortex (DCIC), and external cortex (ECIC) (Nelson et al. 2009). Based on the electrophysiological properties of the recorded neurons (Figs 2 and 3), the IC was classified into three subdivisions (Fig. 3 and Table 1). CIC neurons exhibited fine frequency-tuning (Fig. 3A), short latency (Fig. 3G), low threshold (Fig. 3I), high spontaneous rate (Fig. 3A,D), and sustained temporal response (Fig. 3K) with a well-defined tonotopic organization (Figs 2H and 3I). In contrast to the CIC, neurons in the ECIC (Fig. 3B) and DCIC (Fig. 3C) exhibited broader frequency-tuning (Fig. 3H; CIC and ECIC, $P < 0.0001$; CIC and DCIC, $P < 0.0001$; DCIC and ECIC, $P = 0.096$; one-way ANOVA) with a longer latency (Fig. 3G; CIC and ECIC, $P < 0.0001$;

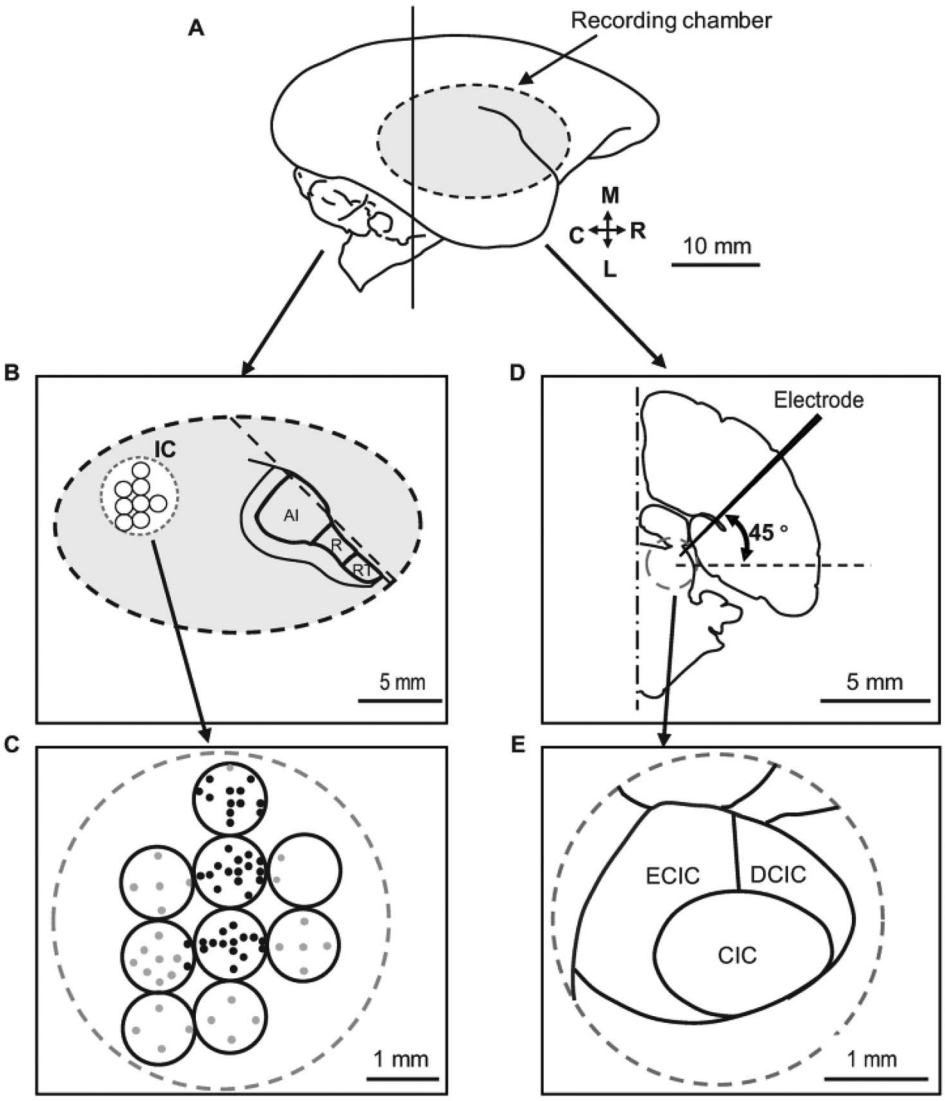

Figure 1. Recording sites in the inferior colliculus of marmosets. (*A*) Lateral view of the right hemisphere of a marmoset. The gray oval indicates the recording chamber built during head-cap implantation. (*B*) Location of the primary auditory cortex (A1) and the inferior colliculus (IC) in the recording chamber of the right hemisphere of a marmoset. The dashed gray circle encloses the mini-craniotomies through which the IC is accessed. AI, primary auditory cortex; R, rostral field; RT, rostral temporal field. (*C*) Penetrations made through the craniotomies shown in *B* to access the IC (black dots penetrations with auditory responses; gray dots, penetrations with no auditory responses). (*D*) Coronal outline along the vertical line in *A* (gray circle, location of the IC). The electrode is advanced in an approximately frontal plane at an angle of 45° lateral to medial to access the IC. (*E*) Subdivisions of the IC in the right hemisphere of a marmoset (CIC, central nucleus of the IC; DCIC, dorsal cortex of the IC; ECIC, external cortex of the IC).

CIC and DCIC, $P = 0.352$; DCIC and ECIC, $P < 0.0001$; one-way ANOVA) and more dynamically changing temporal response profiles as well as a higher response threshold (Fig. 3*I*; CIC and ECIC, $P < 0.001$; CIC and DCIC, $P < 0.0001$; DCIC and ECIC, $P = 0.602$; one-way ANOVA). Consistent with a previous study (Syka et al. 2000), 29% of the IC neurons (64/219) exhibited nonmonotonic rate-level functions in response to the BF tone with different intensities (−10 to 70 dB SPL). The proportion of neurons with nonmonotonic rate-level functions was higher in the CIC than in the ECIC and DCIC (Fig. 3*J*).

Temporal and Rate Representations by IC Neurons

Next, we delivered click trains with varying ICIs (2–100 ms) to investigate the temporal processing by IC neurons in awake marmosets. We found that distinct populations of IC neurons used temporal and/or rate representation to encode click trains. VS and RS were used to quantify the synchronization, whereas the Spearman correlation coefficient was used to quantify their rate-coding properties. The four types of response found previously in the AC (synchronized, mixed, positive-monotonic nonsynchronized, and negative-monotonic nonsynchronized) were also found in the IC (Fig. 4*A–D*). The IC neurons with a synchronized response demonstrated stimulus-synchronized discharges at long ICIs and suppressed firing at short ICIs (Fig. 4*A*, Top). Synchronized neurons showed a large VS and significant RS at long ICIs (Fig. 4*A*, Bottom). IC neurons with a mixed response exhibited stimulus-synchronized discharges at long ICIs, and their firing rate monotonically increased

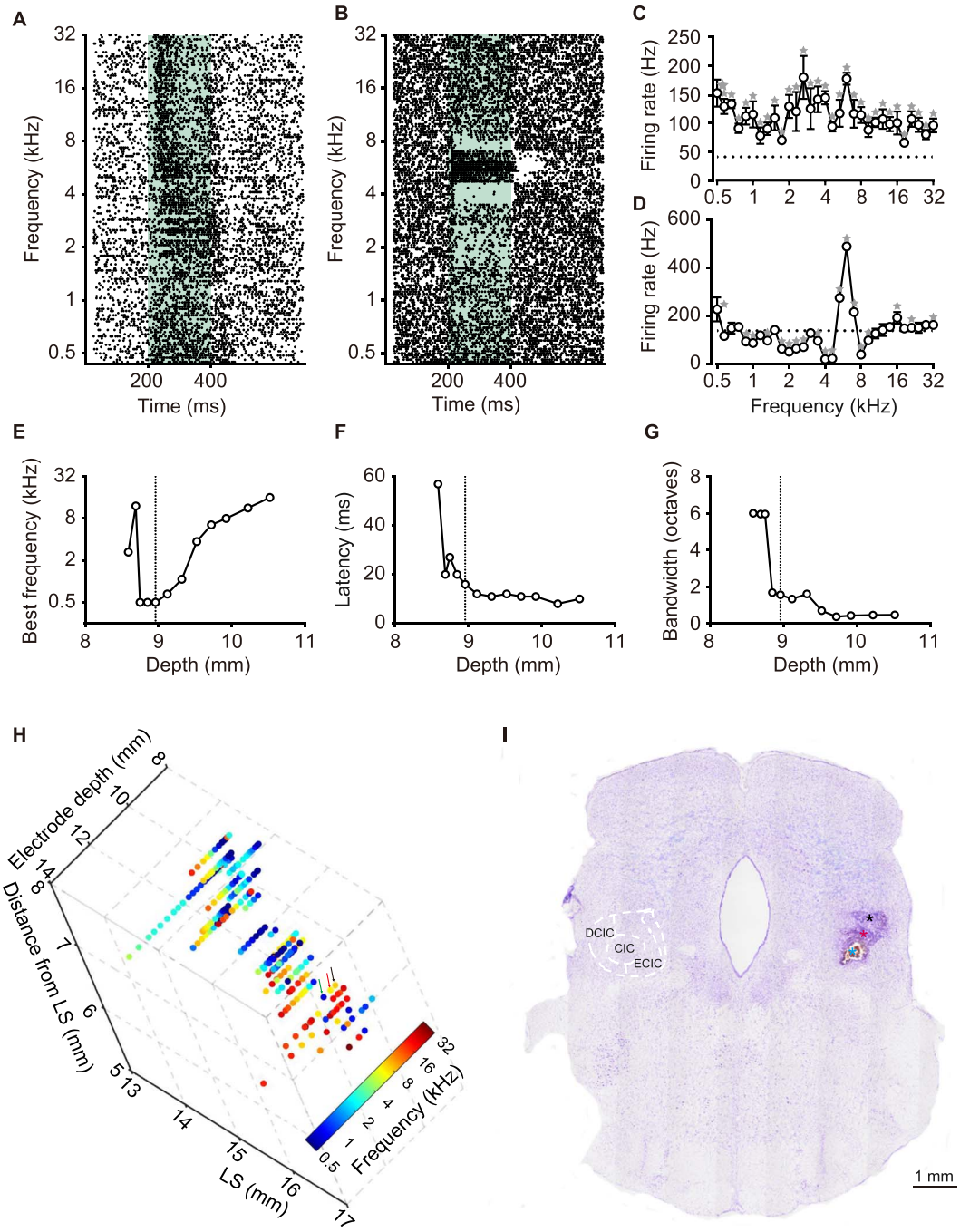

Figure 2. Identification of electrophysiological recording sites in IC. (*A*, *B*) Raster plots of neural responses to pure tones (green shading, periods of acoustic stimulation) in IC. The recording depths are 8589 and 9721 μm, respectively. (*C*, *D*) Frequency tuning curves measured by the firing rate averaged over the duration of the pure tone stimuli (200–400 ms) across five trials for the two example neurons shown in *A* and *B*. The horizontal dashed line indicates the spontaneous firing rate, averaged over the period before the onset of pure tone stimuli (0–200 ms) across five trials. (*E*–*G*) The relationship between the best frequency (*E*), latency (*F*), bandwidth (*G*) and recording depth in a single recording track. The vertical dashed line indicates entry to the CIC subdivision of the IC; before this depth the electrode is in the ECIC subdivision. The best frequency increased with depth in the CIC subdivision. (*H*) Tonotopic map of IC in the right hemisphere of an individual marmoset. The color of the dots represents BF of the recorded neurons. LS, lateral sulcus. The arrows indicate the recorded neurons from the sites in I highlighted with asterisks of same color. (*I*) Image of a Nissl-stained section containing three electrolytic lesions in IC labeled by asterisks of different colors. The outline of IC subdivisions was drawn on the left side of brain slide.

with decreasing ICI (Fig. 4*B*). Strikingly, in contrast to previous studies reporting that almost all IC neurons use stimulus-synchronized responses (temporal representation) to encode the temporal information of sounds (Batra et al. 1989; Wang et al. 2008a, 2008b), we also found a fair number of IC neurons that did not show a stimulus-synchronized spiking response at long ICIs (RS < 13.8). Rather, they demonstrated either an increased (positive-monotonic, Fig. 4*C*) or a decreased firing rate (negative-monotonic, Fig. 4*D* and Supplementary Fig. S1) with increasing ICI, both of which were identified as firing-rate-based nonsynchronized responses. Together,

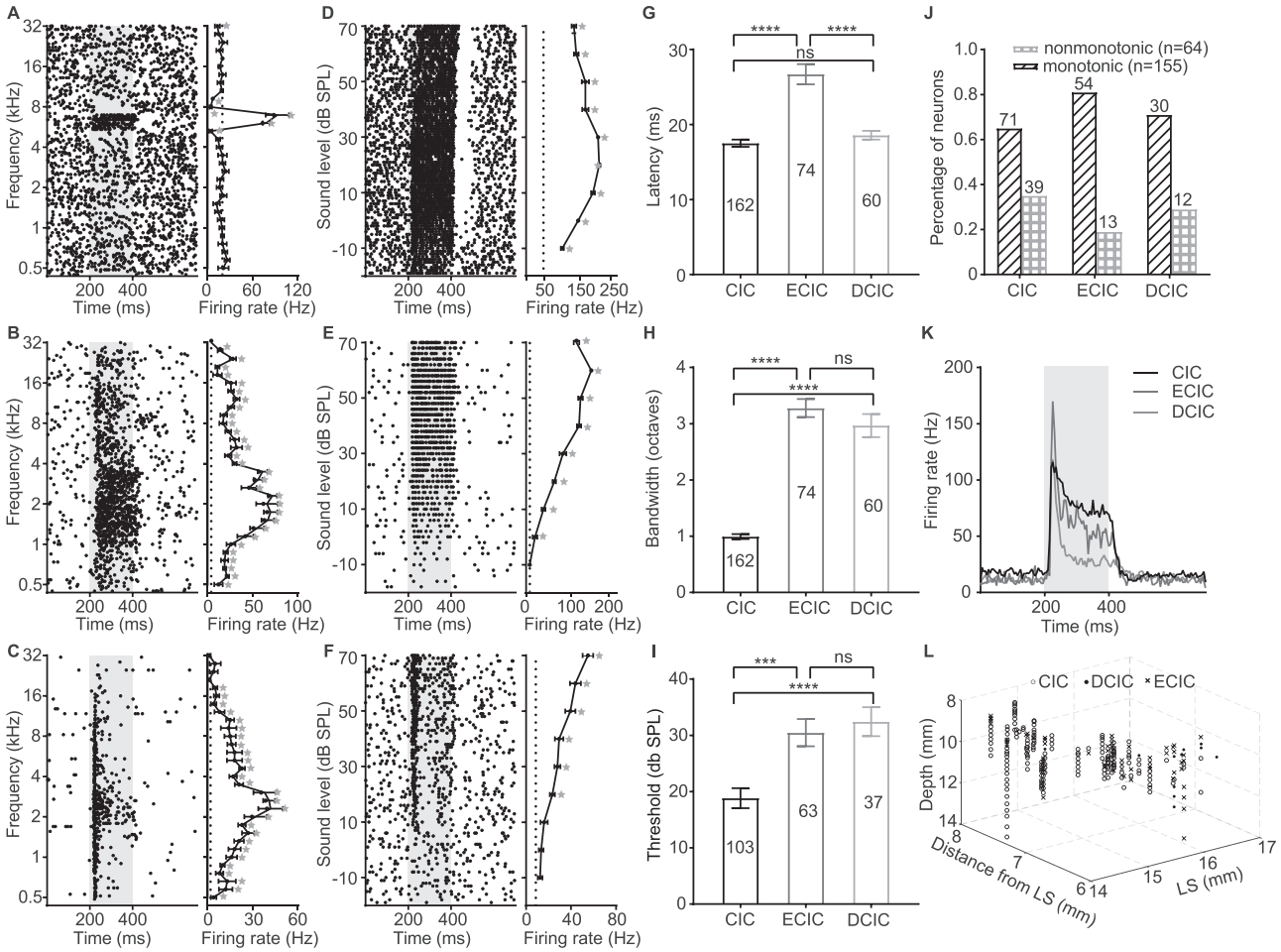

Figure 3. Electrophysiological properties of IC neurons in different subdivisions. (*A–C*) Raster plots (left) of neural responses to pure tones and frequency tuning curves (right) for the example neurons in the CIC, ECIC, and DCIC, respectively. (*D–F*) Raster plots (left) and rate level functions (right) for IC neurons in the CIC, ECIC, and DCIC. Gray shading in *A–F* indicates the onset and duration of the stimulus. (*G–K*) Minimal response latency, half tuning bandwidth, threshold, monotonicity, and mean peristimulus time histograms (PSTHs) of IC neurons in different subdivisions. (*J*) Partition of the IC based on the neural responses. (*L*) Spatial distribution of recorded units in IC subdivisions.

Table 1. Quantification of response properties of CIC, DCIC, and ECIC

Subdivisions of IC	Bandwidth (octaves)	Latency (ms)	Threshold (dB SPL)	Spontaneous rate (spikes/s)
CIC	0.99 ± 0.045	17.51 ± 0.48	18.84 ± 1.78	14.19 ± 1.02
ECIC	3.28 ± 0.16	26.72 ± 1.34	30.48 ± 2.42	13.69 ± 1.94
DCIC	2.97 ± 0.20	18.58 ± 0.58	32.43 ± 2.58	6.75 ± 1.14

we found that IC neurons used both temporal and rate representations to encode time-varying stimuli, which was the same as in the AC.

Distinct Characteristics of Temporal- and Rate-Coding Neurons in the IC

We recorded from a total of 198 typical temporal- and rate-coding neurons in the IC. Of these, 72% used stimulus-synchronized temporal representation (synchronized, 53%; mixed, 19%) and 28% used rate representation (positive-monotonic non-synchronized, 22%; negative-monotonic nonsynchronized, 6%) to encode time-varying stimuli (Fig. 5*A*). To further study the temporal processing in the IC quantitatively, IC neurons with temporal and rate representations were analyzed separately. We found that the VS of synchronized and mixed neurons increased with increasing ICI (Fig. 5*B*). These neurons had best phase-locking responses at long ICIs (Fig. 5*C*). Most of the IC neurons with rate representation were positive-monotonic neurons exhibiting a decreased firing rate with increasing ICI (Fig. 5*D*) and with a Spearman correlation coefficient > 0.4 (Fig. 5*E*). A very small proportion of negative-monotonic nonsynchronized neurons was found in IC, and they showed Spearman correlation coefficients <−0.4 (Fig. 5*E*). To compare

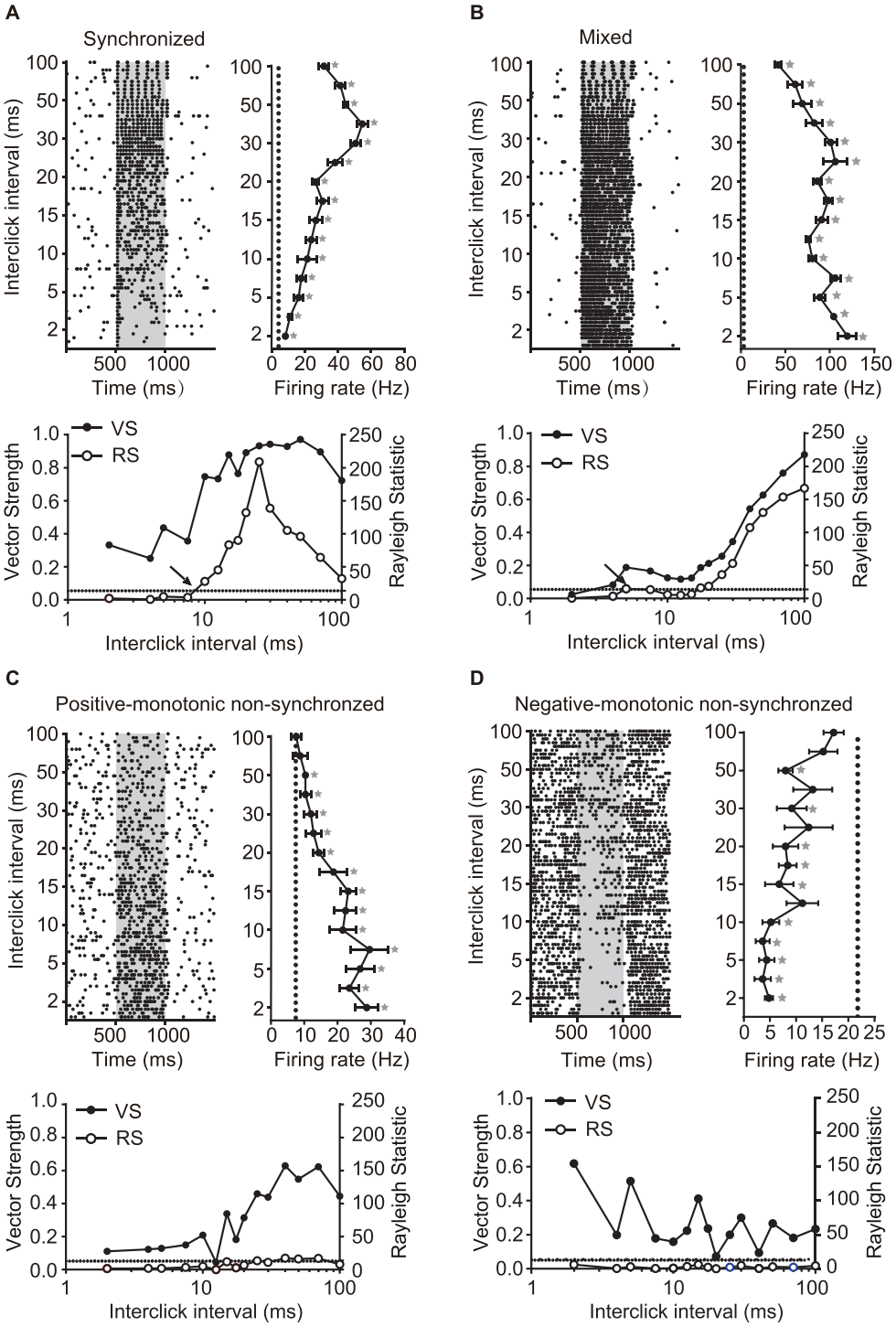

Figure 4. Four types of IC neural responses to Gaussian click trains with varying ICIs. (*A–D*) Example data from IC neurons with stimulus-synchronized (*A*), mixed (*B*), positive-monotonic nonsynchronized (*C*, Spearman correlation coefficient = 0.96), and negative-monotonic nonsynchronized responses (*D*, Spearman correlation coefficient = −0.6). Upper left, raster plots of example IC neurons in response to Gaussian click train with varying ICI (gray shading, periods of acoustic stimulation). Upper right, corresponding firing rates averaged over the duration of the click stimuli (dotted line, mean spontaneous firing rate). Lower panel, vector strength (VS, filled circles) and Rayleigh statistics (RS, blue open circles) of the example neurons in response to click trains (horizontal dashed line at 13.8 indicates significance in Rayleigh statistics, which is equal to $P < 0.001$; arrow, synchronization boundary of the neuron).

with previous studies in AC and MGB consistently, negative-monotonic nonsynchronized neurons were excluded from quantification and statistical tests of nonsynchronized populations, unless otherwise stated. Further analysis revealed that synchronized neurons showed significant RS values (>13.8) and small discharge rate ratio of response to short ICIs versus long ICIs, whereas nonsynchronized neurons showed the opposite characteristics with a large discharge rate ratio and RS values below the threshold for significance (Fig. 5*F*).

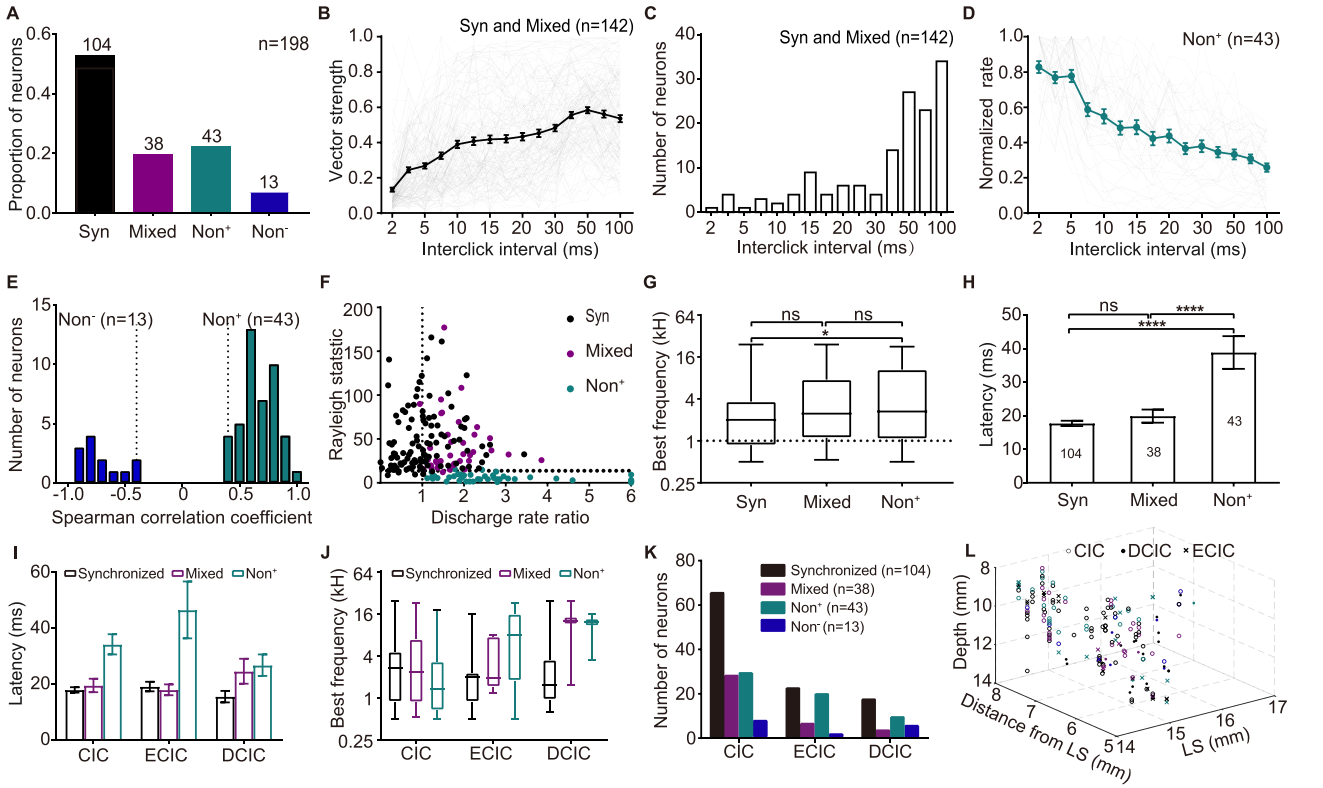

Figure 5. Distinct characteristics of IC neurons with different temporal responses. (*A*) Proportions of IC neurons with synchronized ($n = 104$), mixed ($n = 38$), positive-monotonic ($n = 43$), and negative-monotonic non-synchronized neurons ($n = 13$). (*B*) Mean vector strength of IC neurons with stimulus synchronized and mixed responses (mean ± sem, black) plotted against ICIs. Thin gray lines are the vector strength of individual IC neurons with stimulus synchronized and mixed responses. (*C*) Distribution of ICIs with maximum vector strength in the population of synchronized and mixed neurons. (*D*) The average of normalized firing rate of IC neurons with positive-monotonic nonsynchronized responses as a function of ICI. Thin gray lines are normalized firing rate of individual IC neurons with positive-monotonic nonsynchronized responses. (*E*) Distributions of Spearman correlation coefficients for positive-monotonic (Non^+) and negative-monotonic (Non^-) non-synchronized responses as a function of repetition rate (reciprocal of ICI). (*F*) Characterization of three populations of IC neurons by synchronization and spiking response measures (Y-axis, mean value of the Rayleigh statistic in the 20–100 ms ICI range; horizontal dotted line at 13.8 is statistical significance level of the Rayleigh test ($P < 0.001$); vertical dotted line; discharge rate ratio of 1.0). IC neurons classified as synchronized ($n = 104$), nonsynchronized ($n = 43$), and mixed responses ($n = 38$) are indicated by black, light gray, and dark gray, respectively. (*G*) Best frequencies of IC neurons with synchronized, mixed, and positive-monotonic non-synchronized responses. The value of best frequency is the base 2 logarithm. (*H*) Minimal response latencies of IC populations with synchronized, positive-monotonic nonsynchronized, and mixed responses. (*I*) Minimal response latencies of CIC, ECIC, and DCIC neurons with synchronized, positive-monotonic nonsynchronized, and mixed responses. (*J*) Best frequencies of CIC, ECIC, and DCIC neurons with synchronized, mixed, and positive-monotonic non-synchronized responses. (*K*) Proportion of IC neurons with synchronized, mixed, and nonsynchronized (positive-monotonic and negative monotonic) responses in IC subdivisions. (*L*) Distribution of IC neurons with synchronized, mixed, and nonsynchronized (positive-monotonic and negative monotonic) responses in IC subdivisions.

Thus, synchronized, nonsynchronized, and mixed neurons were roughly separated into three populations when their RS values were plotted against the discharge rate ratios of response to short ICIs versus long ICIs (Fig. 5*F*). We also found that positive-monotonic nonsynchronized neurons had higher BFs (Fig. 5*G*; synchronized and mixed, $P = 0.144$, synchronized and non$^+$, $P = 0.028$, mixed and non$^+$, $P = 0.579$, one way ANOVA) and longer response latencies (Fig. 5*H*; Synchronized and Mixed, $P = 0.596$; Synchronized and Non$^+$, $P < 0.001$; Mixed and Non$^+$, $P < 0.001$; one way ANOVA) compared with neurons with stimulus-synchronized responses. We further compared these response properties of synchronized, mixed, and positive-monotonic non-synchronized neurons among IC subdivisions. No significant difference was found in response latency (Fig. 5*I*, $F = 0.816$, $P = 0.444$, two-way ANOVA). BF of the positive-monotonic non-synchronized neurons in DCIC was higher than in ECIC and CIC (Fig. 5*J*, $F = 3.515$, $P = 0.046$; two-way ANOVA). As for the spatial locations, IC neurons with temporal and rate representations did not show distinct distributions in IC subdivisions (Fig. 5*K*,*L*, Table 2).

Temporal-to-Rate Transformation from Midbrain to Cortex

To understand the temporal processing along the auditory afferent pathway, we compared our IC data with those in the MGB and AC of the same species (Lu et al. 2001a, 2001b; Bartlett and Wang 2007). In contrast to the AC, a larger proportion of IC neurons used stimulus-synchronized temporal representation to encode time-varying stimuli, the proportion of which decreased from the IC to the AC, whereas those with rate representation increased from the IC to the AC (Fig. 6*A*). This result echoes the view of a temporal-to-rate transformation of

Table 2. Quantification of IC neurons with different temporal response types

Temporal response type	Latency (ms)	Best frequency (kHz)	Spontaneous rate (spikes/s)
Syn ($n = 104$)	17.70 ± 0.79	3.55 ± 0.44	15.81 ± 1.5
Mixed ($n = 38$)	19.89 ± 1.99	4.96 ± 0.92	20.45 ± 2.75
Non-syn ($n = 43$)	38.86 ± 4.86	6.46 ± 1.03	7.83 ± 1.44

temporal processing along the ascending auditory pathway (Wang et al. 2008a, 2008b). However, our results differ from the previous study which reported that 100% of IC neurons show temporal representation (Wang et al. 2008a, 2008b). The MGB has been reported to have the highest proportion of mixed neurons with a combination of temporal and rate coding (Fig. 6A). It is hard to explain the mixed neurons with a combination of temporal and rate coding in MGB by temporal information flow in the ascending auditory pathway alone, and cortical feedback projections may play a critical role (Wang et al. 2008a, 2008b). The synchronization boundary has been applied to quantify the synchronization of auditory neurons (Wang et al. 2008a, 2008b). Therefore, we compared the synchronization boundary of neurons with temporal representation in the IC, MGB, and AC (Fig. 6B). The highest proportion of IC neurons tended to synchronize with a fast temporal rate (ICI = 5 ms; repetition rate = 200 Hz), much higher than that in the AC (ICI > 25 ms; repetition rate < 40 Hz). The median synchronization boundary of IC neurons was 5.6 ms, in contrast to 5.2 ms for MGB neurons (Bartlett and Wang 2007) and 21.3 ms for AC neurons (Lu et al. 2001a, 2001b). Thus, our results combined with previous studies in the MGB and A1 of awake marmosets indicate that there is a smaller degree of temporal-to-rate transformation from the midbrain to the AC (Fig. 6C). However, the auditory station at which rate representation emerged was much earlier than the speculation in a previous report (Wang et al. 2008a, 2008b).

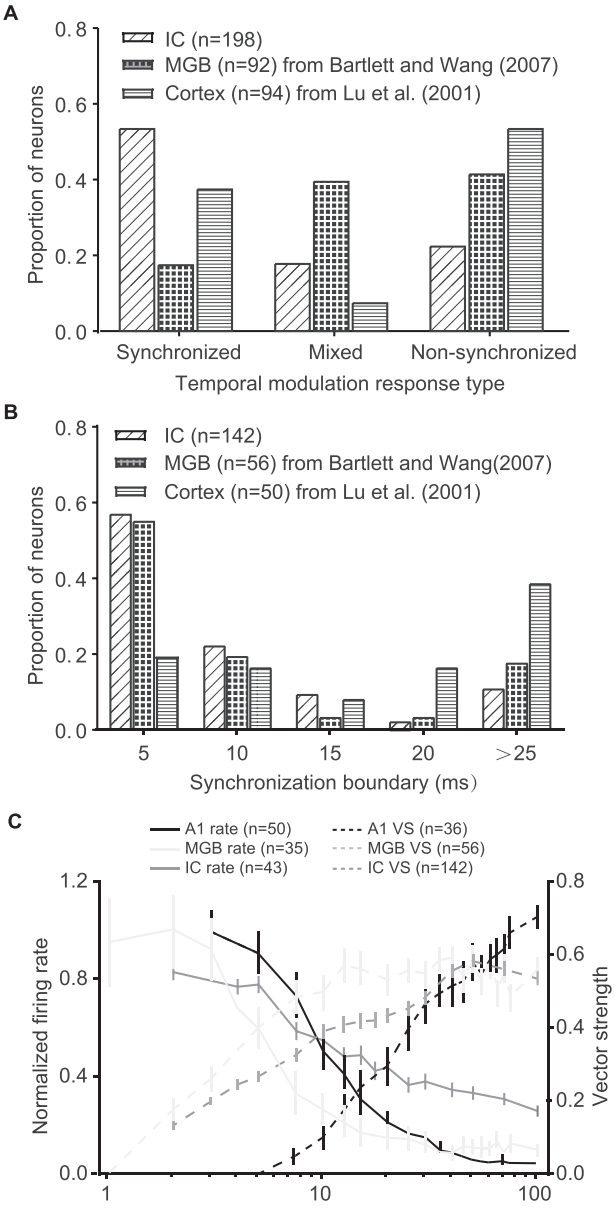

Figure 6. Comparison of temporal and rate representation in the IC, MGB, and cortex. (*A*) Proportions of synchronized, mixed, and non-synchronized neurons in the IC, MGB, and cortex. (*B*) Distribution of synchronization boundaries in the IC, MGB, and cortex. Data for the IC are from this study, data for the MGB are from Bartlett and Wang (2007), and data for the auditory cortex are from Lu et al. (2001b). (*C*) Comparison of temporal and rate representations in IC, MGB, and A1. Stimulus-synchronized spiking responses are quantified by VS. Nonsynchronized responses are quantified by the normalized firing rate. Error bars represent standard error of the mean (SEM). Data for the IC are from this study, data for the MGB are from Bartlett and Wang (2007), and data for the auditory cortex are from Lu et al. (2001b).

Inactivation of A1 Changes the Tuning Properties of IC Neurons

As cortical feedback projections are extensive (Nunez and Malmierca 2007), and modulate many aspects of sound-processing by IC neurons (Bajo et al. 2010), we wondered whether cortical feedback projections modulate temporal processing in the IC of awake marmoset. To address this question, we recorded the responses of IC neurons to time-varying stimuli before, during, and after inactivation of A1 reversibly via a cryoloop (Fig. 7A,B). We validated the effectiveness of our cooling system by positioning a cryoloop with a temperature sensor on the surface of A1 of anesthetized rats. We found that white broadband noise elicited spiking responses vanished when the temperature fell to 3 °C and were restored when the temperature was raised back to a normal temperature (Supplementary Fig. S2A–B). The inactivated brain area via a cryoloop was within 2.5 × 2.5 mm in distance and depth at a loop temperature of 3 °C (Supplementary Fig. S2C–J). Similar to the results in anesthetized rats, spiking activity adjacent to the cryoloop of awake marmosets was totally blocked when the temperature fell to 3 °C and restored at normal temperature (Fig. 7C).

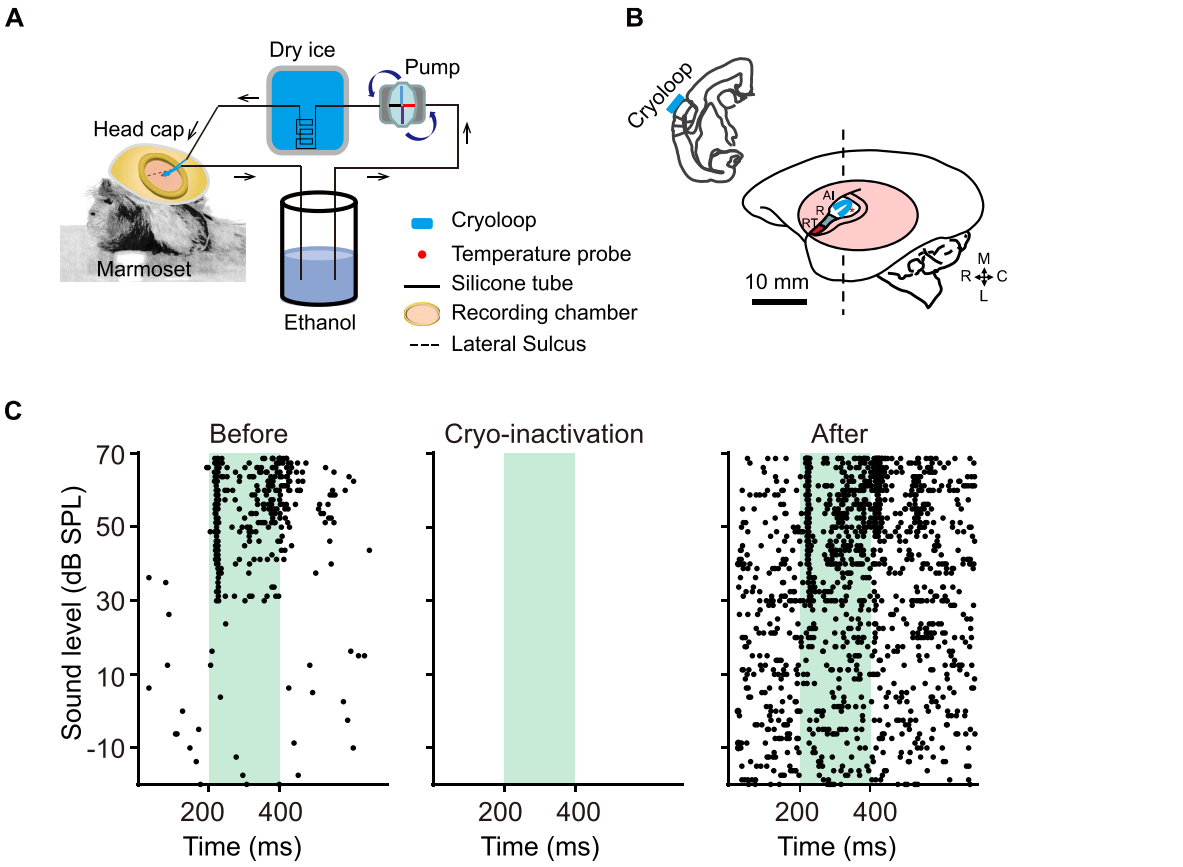

Figure 7. Cooling method for inactivation of A1 in awake marmosets. (*A*) Schematic of the cooling device. Flow rate is adjusted by the pump. Arrows indicate direction of fluid flow. The red dot shows the position of the temperature probe; the indigo rectangle is the cryoloop; the dashed line indicates the lateral sulcus; the pink oval indicates the recording chamber. (*B*) Sketch of the location of A1 and relative position of the cryoloop (U-shaped) in the left hemisphere of a marmoset. The core regions of the auditory cortex are presented in different colors: primary auditory cortex (A1) and rostral fields (R and RT). The pink oval indicates the position of the recording chamber. The dashed vertical line shows the position for the coronal section in the upper left illustration, in which the blue rectangle indicates the position of the cryoloop. The red star is the location for neural recording in *C*. R, rostral; C, caudal; M, medial; L, lateral. Scale bar: 10 mm. (*C*) Validation of cooling effects near the cryoloop. The recording sites (recording depth: 1437 μm) are highlighted by red stars in *B*. Raster plots showing the neural spiking responses to white broad-band noise (WB) with different sound levels before, during, and after inactivation of A1 (green shading, periods of acoustic stimulation).

First, we examined the tuning properties of IC neurons before and during inactivation of A1. We found that both the response to tones and the temporal firing pattern of IC neurons changed during A1 inactivation (Fig 8*A*,*B*), especially the responses to the BF tone: The BF and the tuning bandwidth changed (Fig. 8*C*). We compared the firing rate of IC neurons in response to the BF tone before and during A1 inactivation and found a significant decrease (Fig. 8*D*, $P = 0.0014$, paired *t*-test), indicating that A1 enhanced IC neural responses in the awake state. Examination of the frequency tuning of 43 IC neurons before and during A1 inactivation revealed that the BF changed in more than half of them (23/43), and two-thirds showed either an increased (14/43) or decreased (16/43) tuning bandwidth during A1 inactivation (Fig. 8*E*,*F*). Our results demonstrate that A1 modulates the frequency-tuning of IC neurons in awake marmosets, which is consistent with previous studies in other species (Zhang et al. 1997; Zhou and Jen 2007).

Temporal and Rate Coding of IC Neurons during Inactivation of A1

Because firing-rate-based nonsynchronized response to time-varying signals has mainly been found in the AC of awake animals (Bendor and Wang 2007; Dong et al. 2011; Gao and Wehr 2015; Gao et al. 2016), we wondered whether the rate representation we found in the IC of awake marmosets was due to a cortico–colliculus feedback projection. To answer this question, we examined the changes in the synchronized and nonsynchronized responses of IC neurons before, during, and after inactivation of A1 by cryoloop. As shown by the example in Figure 9A, although its firing rate in stimulus-synchronized responses decreased slightly during inactivation of A1 (Fig. 9C left), its VS and RS did not change significantly during the inactivation of A1 (Fig. 9C middle and right). For most IC neurons with a positive-monotonic nonsynchronized response that exhibited a decreased firing rate with increasing ICIs (Fig. 9*B*,*D*), although the firing rate of this example

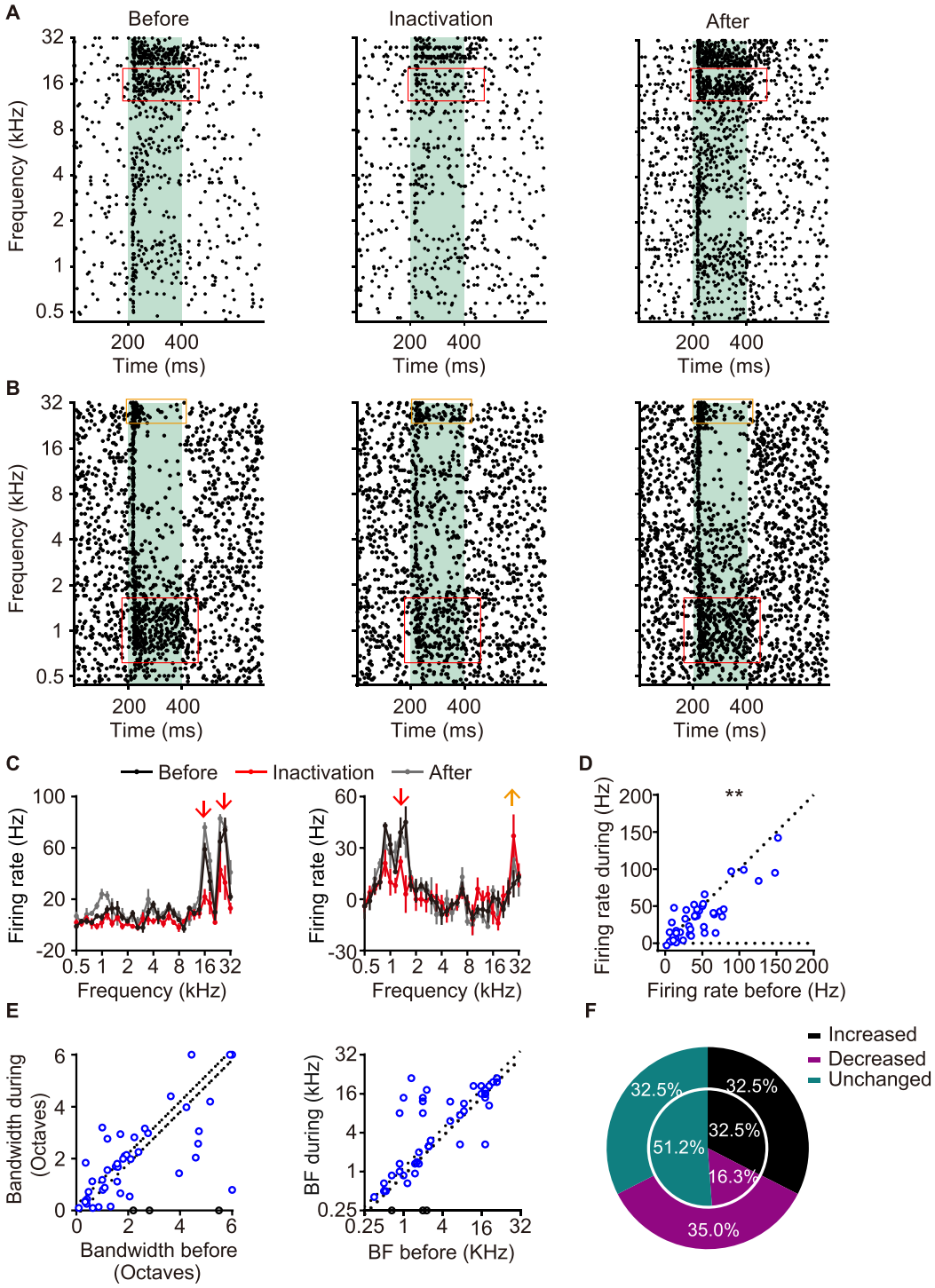

Figure 8. Inactivation of A1 Modulates the Frequency Tuning of IC Neurons. (*A*, *B*) Raster plots of two example IC neurons in response to pure tones with varying frequencies before (left), during (middle), and after (right) inactivation of A1 (green shading, periods of acoustic stimulation; red boxes, the tone-evoked response changes greatly during A1 inactivation). (*C*) Frequency tuning curves of example IC neurons shown in *A* before, during, and after inactivation of A1 (arrows, increasing or decreasing trend of the response). (*D*) Firing rate in response to the BF tone before A1 inactivation plotted against that during A1 inactivation for 46 IC neurons. (*E*) BF (left) and half tuning bandwidth (right) of IC neurons before inactivation of A1 plotted against those during A1 inactivation. The dashed lines indicate the confidence interval (0.2 octaves). (*F*) Proportions of IC neurons exhibiting increased, decreased, and unchanged tuning bandwidth (outer circle) or BF (inner circle) as shown in *E*.

neuron in response to fast click trains decreased slightly, the curve of firing rates plotted against ICIs did not change significantly during A1 inactivation (Fig. 9D, left). To further quantify these results, we first compared the firing rates of IC neurons with different temporal responses (synchronized, positive monotonic, negative monotonic, nonsynchronized, and mixed) before and during A1 inactivation, and found that the rate significantly decreased during A1 inactivation (Fig. 10A, $P < 0.0001$, paired *t*-test). Second, we compared the

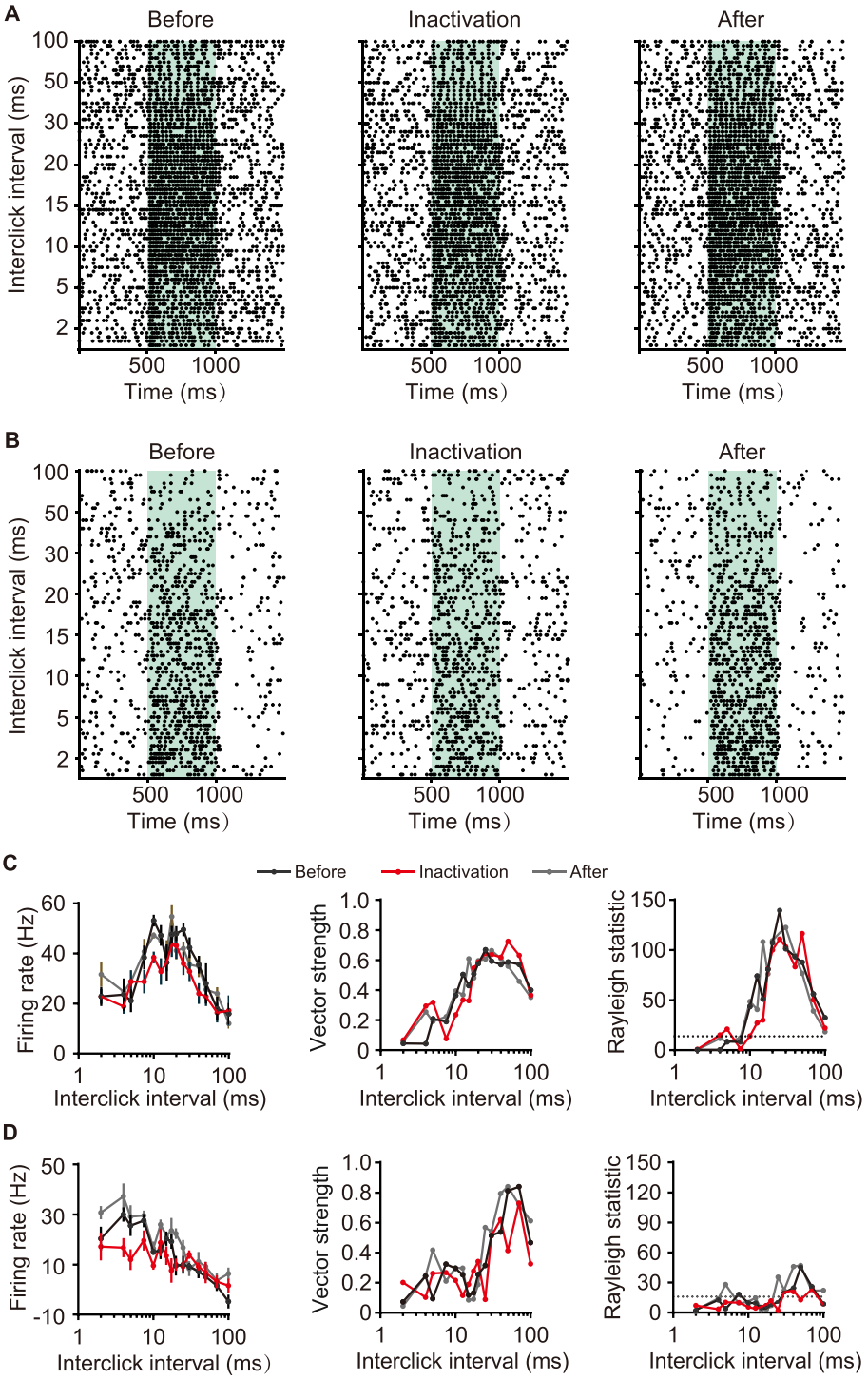

Figure 9. IC Synchronized and Nonsynchronized Responses before and during Inactivation of A1. (*A*, *B*) Raster plot of example IC neurons with stimulus-synchronized (*A*) and positive-monotonic nonsynchronized responses (*B*) in response to Gaussian click trains with varying ICIs before, during, and after A1 inactivation (green shading, the onset and duration of the stimulus). (*C*, *D*) Firing rate (left), vector strength (middle), and Rayleigh statistics (right) of the example IC neurons in *A* and *B* before, during, and after A1 inactivation (the value of the horizontal dashed line in the right plot is 13.8).

maximal VS of IC neurons with temporal representation (synchronized and mixed responses), and found no significant difference (Fig. 10*B*, $P = 0.557$, paired *t*-test). In these neurons, we further compared the VS across different ICIs before and during A1 inactivation, which showed that 4 out of 23 displayed a significant difference (Fig. 10*E*, $P < 0.05$, paired *t*-test). In the 24 neurons showing a decreased firing rate with increasing ICIs, when we compared their Spearman correlation coefficients (Fig. 10*C*, $P = 0.08$, paired *t*-test) as well as the discharge rate ratios in response to short ICIs versus long ICIs (Fig. 10*D*, $P = 0.385$, paired *t*-test) before and during A1 inactivation, 5 out of 24 neurons showed a significant change (Fig. 10*E*). Our results indicate

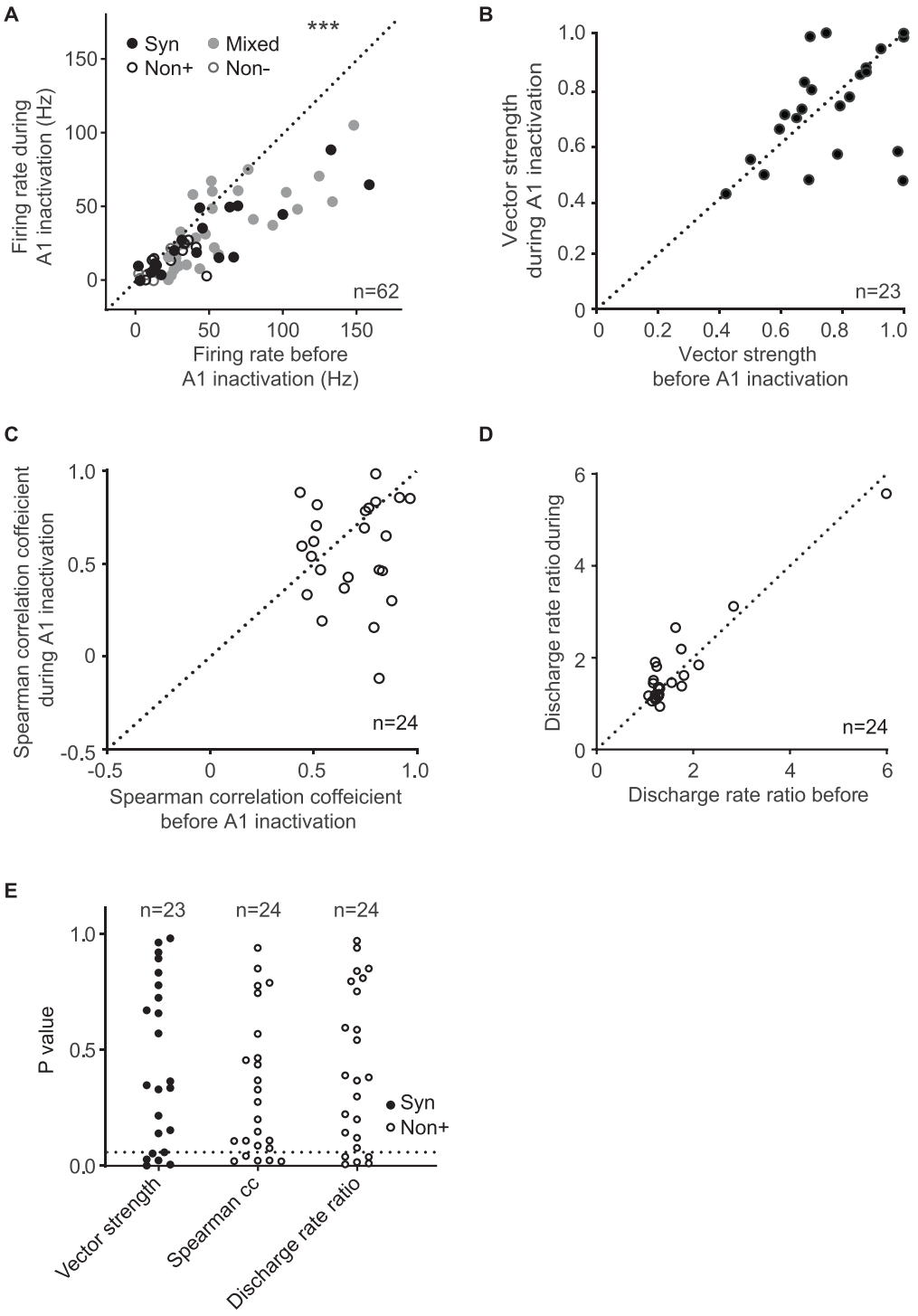

Figure 10. Quantitative Analysis of Changes in Temporal and Rate Representation Caused by A1 Inactivation. (*A*) Firing rates of IC neurons with different temporal responses before and during A1 inactivation (***$P < 0.001$, student's paired *t* test). (*B*) Comparison of maximal vector strength of synchronized and mixed neurons in response to certain ICIs before A1 inactivation with those during A1 inactivation. (*C*) Comparison of Spearman correlation coefficients of firing rate across the ICIs of non-synchronized neurons before A1 inactivation with those during A1 inactivation. (*D*) Comparison of discharge rate ratio at short ICIs versus long ICIs of non-synchronized neurons before A1 inactivation with those during A1 inactivation. (*E*) *P* values of Student's paired *t* test for vector strength of synchronized neurons before and during A1 inactivation as well as Spearman correlation coefficients and discharge rate ratios of nonsynchronized neurons before and during A1 inactivation (dashed line, 0.05).

that cortico-colliculus descending projections mainly modulate the response magnitude of IC neurons and influence the temporal processing by IC neurons (Fig. 10).

Discussion

In this study, we used single-unit recordings to study temporal processing in the IC of awake marmosets and further determined whether and how cortical feedback

projections modulate this processing by reversibly inactivating the AC. We found that IC neurons use not only temporal but also rate representation to encode time-varying stimuli at the millisecond scale. Moreover, we showed that rate representation by IC neurons was largely not due to cortical feedback projections. Our study revealed that the emergence of nonsynchronized responses occurred as early as the midbrain and that a temporal-to-rate transformation gradually changed along the ascending auditory pathway.

Advantage and Disadvantage of the Cooling Technique

In comparison with other methods, for example, physical lesions (Neff and Casseday 1977), the pharmacological method (Smith et al. 2004), optogenetics (Yao et al. 2012; Warden et al. 2014; Moser 2015; Xu et al. 2016), and chemical-genetics (Roth 2016), cooling is the first choice for us to inactivate the A1 of awake marmosets as its effects are acute and reversible (Lomber et al. 1999). It is particularly advantageous for manipulating large areas of brain tissue, especially those of nonhuman primates, for which genetic tools have not been well-developed yet (Plakke et al. 2015; Dash et al. 2018). Moreover, cooling is the most commonly used method to demonstrate causal relationships between a particular brain region and behavioral performance (Lomber et al. 1996; Malhotra and Lomber 2007; Wood et al. 2017). However, the extent of inactivation needs to be assessed by electrophysiological, thermal or metabolic measures (Lomber et al. 1999), and cell type specific inactivation cannot be precisely achieved by the cooling method.

Temporal and Rate Representations in the Central Auditory Pathway

Previous studies have demonstrated that cortical neurons use either temporal or rate representation to encode time-varying stimuli at the millisecond scale (Lu et al. 2001a, 2001b; Bendor and Wang 2007; Gao et al. 2016). Temporal representation has been found in each station along the ascending auditory pathway, which shows gradually decreasing synchronization (Joris et al. 2004; Wang et al. 2008a, 2008b). Intracellular studies have shown that the membrane potential of cortical stimulus-synchronized neurons phase-lock to higher repetition rates than the spiking response, demonstrating decreased synchronization from inputs to output in synchronized cortical neurons (Gao et al. 2016). Rate representation has mainly been found in the AC of awake animals (Lu et al. 2001a, 2001b) and later in the MGB of awake marmosets (Bartlett and Wang 2007). In this study, we found that 28% of IC neurons displayed rate representation with non-synchronized responses (Figs 4C,D and 5A).

Our results combined with previous studies (Lu et al. 2001a, 2001b; Bendor and Wang 2007) revealed that temporal and rate representations of time-varying stimuli at the millisecond scale may be ubiquitous from midbrain to AC (Fig. 6). Most notable, rate representation may emerge earlier than the IC, which, however, needs to be further investigated in awake animals. Our study showed that IC neurons with rate representation have higher BFs than those with synchronized responses (Fig. 5G), suggesting that IC neurons with low BFs prefer stimulus-synchronized temporal code whereas those with high BFs prefer firing-rate-based rate code to encode time-varying stimuli. The response latencies of IC neurons with non-synchronized responses were much longer than those with mixed and synchronized responses (Fig. 5H), which is consistent with the findings in the AC (Bendor and Wang 2007; Gao et al. 2016).

Temporal-To-Rate Transformation along the Ascending Auditory Pathway

Temporal and rate representations of time-varying stimuli have been extensively studied in the AC of awake animals (Lu et al. 2001a, 2001b; Bendor and Wang 2007; Gao and Wehr 2015; Gao et al. 2016). Extracellular studies have demonstrated transformation from temporal to rate representation from the A1 to higher-order cortex: the rostral fields (rostral and rostral temporal) (Bendor and Wang 2007). Within A1, intracellular studies have shown that nonsynchronized neurons receive synchronized inputs (Gao et al. 2016), suggesting that the temporal-to-rate transformation may occur from the MGB to A1. The current study in the IC of awake marmoset, together with previous studies in the MGB and AC of the same species, indicated that the proportion of auditory neurons with temporal representation gradually decreased whereas those with rate representation gradually increased (Fig. 6A), revealing the temporal-to-rate transformation from midbrain to cortex *via* the auditory thalamus. In addition, we found that the proportion of auditory neurons with monotonic rate level function gradually decreased along the ascending auditory pathway (IC, 70.8%; MGB, 22%; A1, 20–40%) although neurons with monotonic and nonmonotonic rate level functions did not show specific distribution among IC and MGB subdivisions as well as within the core areas of the auditory cortex (Bendor and Wang 2008; Bartlett and Wang 2011).

Opponent Rate-Coding Is Not Unique in the AC

Previous studies have shown that the AC has two distinct populations (positive-monotonic and negative-monotonic) of nonsynchronized neurons (Bendor and Wang 2007; Gao et al. 2016), which are thought to use the opponent rate-coding principle to encode rapidly changing time-varying stimuli (Bendor and Wang 2007; Gao et al. 2016; Petkov and Bendor 2016), which is distinct from the neural coding of sound levels and other sound features (Petkov and Bendor 2016). Surprisingly, in this study, we found two distinct populations of nonsynchronized neurons in the IC. These results

suggest that the IC may also use the opponent rate-coding principle to encode rapidly changing time-varying stimuli that cannot be faithfully replicated by stimulus-synchronized responses. As the opponent rate-coding was only observed in the IC and the sensory cortex of awake non-human primates (Salinas et al. 2000; Bendor and Wang 2007; Gao et al. 2016), it remains unknown whether it is species specific.

Potential Mechanisms Underlying Rate Representation in the IC

The central auditory system, like other sensory systems, consists of efferent pathways in parallel with their corresponding afferent pathways (Nunez and Malmierca 2007). Previous studies have shown that the IC receives a wide range of cortical feedback projections. The DCIC and ECIC are the principal targets of corticocollicular axons (Herbert et al. 1991; Saldana et al. 1996; Druga et al. 1997; Winer et al. 1998). Projections to the CIC has also been reported in some studies, which is the direct, tonotopically organized projections from the primary auditory cortex (Bajo and Moore 2005; Bajo et al. 2007; Malmierca et al. 2008; Bajo and King 2012; Markovitz et al. 2013). Thus, there may be several different pathways via which the cortex could modulate IC neurons. Corticofugal projections have been found to modulate the spectral, intensity, and spatial aspects of auditory processing by IC neurons (Yan and Ehret 2002; Popelar et al. 2003; Bajo and King 2012; Suga 2020). However, little is known about the cortico-collicular modulation of temporal processing. Here, we examined temporal processing in the IC of awake marmosets before and during reversible inactivation of A1 using a cryoloop. We found that inactivation of A1 did not substantially change the temporal processing of IC neurons, although the firing rates decreased during inactivation (Figs 9 and 10). Our results revealed that rate representation by IC neurons was not due to cortical feedback projections, which may emerge earlier than the IC or generate within IC local circuitry. More work is required to test these possibilities.

Several computational models proposed for the AC (Gao et al. 2016; Lee et al. 2020) may shed light on the neuronal mechanisms underlying the generation of temporal response types in IC. In these models based on the leaky integrate-and-firing model, some key parameters were found critical to producing the temporal response schemes of AC, such as the temporal delay of excitatory and inhibitory inputs; the ratio of the strength of excitatory to the inhibitory input, synaptic time constant, stimulus-evoked short-term depression, and so on. The single-neuron models proposed for AC may be largely applicable to the IC except the negative monotonic non-synchronized neurons. As the firing rate of these neurons was below the spontaneous rate, which is quite different from that in AC with increased firing rate at lower click rates. Thus the negative monotonic nonsynchronized neuron of IC may have distinct neural mechanism from that of the AC. They may receive inhibitory inputs from other IC neurons with a positive-monotonic rate profile. More study is required to test the hypothesis.

In summary, our data showed that IC neurons use dual temporal and rate representation to encode time-varying stimuli at the millisecond scale and the rate representation by IC neurons may inherit this property from a lower-level auditory station or generate it with IC local circuitry.

Supplementary Material

Supplementary material can be found at *Cerebral Cortex* online.

Funding

National Natural Science Foundation of China (31871056, 61703365 and 91732302); the MOE Frontier Science Center for Brain Science & Brain-Machine Integration, Zhejiang University, Fundamental Research Funds for the Central Universities (2018QN81008 and 2019XZZX001-01-20); and the National Key R&D Program of China (2018YFC1005003).

Notes

We are indebted to Anna Wang Roe for her valuable suggestions. *Conflict of Interest:* The authors declare that they have no competing financial interests.

References

Aitkin L, Tran L, Syka J. 1994. The responses of neurons in subdivisions of the inferior colliculus of cats to tonal, noise and vocal stimuli. *Exp Brain Res*. 98:53–64.

Bajo VM, King AJ. 2013. Cortical modulation of auditory processing in the midbrain. *Front Neural Circuits*. 6:114.

Bajo VM, Moore DR. 2005. Descending projections from the auditory cortex to the inferior colliculus in the gerbil, *Meriones unguiculatus*. *J Comp Neurol*. 486:101–116.

Bajo VM, Nodal FR, Bizley JK, Moore DR, King AJ. 2007. The ferret auditory cortex: descending projections to the inferior colliculus. *Cereb Cortex*. 17:475–491.

Bajo VM, Nodal FR, Moore DR, King AJ. 2010. The descending corticocollicular pathway mediates learning-induced auditory plasticity. *Nat Neurosci*. 13:253–260.

Bartlett EL, Wang X. 2007. Neural representations of temporally modulated signals in the auditory thalamus of awake primates. *J Neurophysiol*. 97:1005–1017.

Bartlett EL, Wang X. 2011. Correlation of neural response properties with auditory thalamus subdivisions in the awake marmoset. *J Neurophysiol*. 105:2647–2667.

Batra R, Kuwada S, Stanford TR. 1989. Temporal coding of envelopes and their interaural delays in the inferior colliculus of the unanesthetized rabbit. *J Neurophysiol*. 61:257–268.

Bendor D, Wang X. 2007. Differential neural coding of acoustic flutter within primate auditory cortex. *Nat Neurosci*. 10:763–771.

Bendor D, Wang X. 2008. Neural response properties of primary, rostral, and rostrotemporal core fields in the auditory cortex of marmoset monkeys. *J Neurophysiol*. 100:888–906.

Blackwell JM, Lesicko AM, Rao W, de Biasi M, Geffen MN. 2020. Auditory cortex shapes sound responses in the inferior colliculus. *Elife*. 9:1–26.

Creutzfeldt O, Hellweg FC, Schreiner C. 1980. Thalamocortical transformation of responses to complex auditory stimuli. *Exp Brain Res*. 39:87–104.

Dash S, Peel TR, Lomber SG, Corneil BD. 2018. Frontal eye field inactivation reduces saccade preparation in the superior colliculus but does not Alter how preparatory activity relates to saccades of a given latency. *Eneuro*. 5:ENEURO.0024–ENEU18.2018.

de Ribaupierre F, Rouiller E, Toros A, de Ribaupierre Y. 1980. Transmission delay of phase-locked cells in the medial geniculate body. *Hear Res*. 3:65–77.

Ding N, Patel AD, Chen L, Butler H, Luo C, Poeppel D. 2017. Temporal modulations in speech and music. *Neurosci Biobehav Rev*. 81: 181–187.

Dong C, Qin L, Liu Y, Zhang X, Sato Y. 2011. Neural responses in the primary auditory cortex of freely behaving cats while discriminating fast and slow click-trains. *PLoS One*. 6:e25895.

Druga R, Syka J, Rajkowska G. 1997. Projections of auditory cortex onto the inferior colliculus in the rat. *Physiol Res*. 46:215–222.

Eguia MC, Garcia GC, Romano SA. 2010. A biophysical model for modulation frequency encoding in the cochlear nucleus. *J Physiol Paris*. 104:118–127.

Epping WJ, Eggermont JJ. 1986. Sensitivity of neurons in the auditory midbrain of the grassfrog to temporal characteristics of sound. II. Stimulation with amplitude modulated sound. *Hear Res*. 24: 55–72.

Frisina RD, Smith RL, Chamberlain SC. 1990. Encoding of amplitude modulation in the gerbil cochlear nucleus: I. A hierarchy of enhancement. *Hear Res*. 44:99–122.

Gao L, Kostlan K, Wang Y, Wang X. 2016. Distinct subthreshold mechanisms underlying rate-coding principles in primate auditory cortex. *Neuron*. 91:905–919.

Gao L, Wang X. 2019. Subthreshold activity underlying the diversity and selectivity of the primary auditory cortex studied by intracellular recordings in awake marmosets. *Cereb Cortex*. 29:994–1005.

Gao L, Wang X. 2020. Intracellular neuronal recording in awake nonhuman primates. *Nat Protoc*. 15:3615–3631.

Gao PP, Zhang JW, Fan SJ, Sanes DH, Wu EX. 2015. Auditory midbrain processing is differentially modulated by auditory and visual cortices: an auditory fMRI study. *Neuroimage*. 123: 22–32.

Gao X, Wehr M. 2015. A coding transformation for temporally structured sounds within auditory cortical neurons. *Neuron*. 86: 292–303.

Goldberg JM, Brown PB. 1969. Response of binaural neurons of dog superior olivary complex to dichotic tonal stimuli: some physiological mechanisms of sound localization. *J Neurophysiol*. 32: 613–636.

Gruters KG, Groh JM. 2012. Sounds and beyond: multisensory and other non-auditory signals in the inferior colliculus. *Front Neural Circuit*. 6:6–96. https://doi.org/10.3389/fncir.2012.00096.

Hardman C, Ashwell K. 2012. *Stereotaxic and chemoarchitectural atlas of the brain of the common marmoset (Callithrix jacchus)*. 1st ed. CRC Press. https://doi.org/10.1201/b11635.

Heil P, Peterson AJ. 2017. Spike timing in auditory-nerve fibers during spontaneous activity and phase locking. *Synapse*. 71:5–36.

Herbert H, Aschoff A, Ostwald J. 1991. Topography of projections from the auditory cortex to the inferior colliculus in the rat. *J Comp Neurol*. 304:103–122.

Joris PX, Schreiner CE, Rees A. 2004. Neural processing of amplitude-modulated sounds. *Physiol Rev*. 84:541–577.

Joris PX, Smith PH, Yin TC. 1994. Enhancement of neural synchronization in the anteroventral cochlear nucleus. II. Responses in the tuning curve tail. *J Neurophysiol*. 71:1037–1051.

Karklin Y, Ekanadham C, Simoncelli EP. 2012. Hierarchical spike coding of sound. *Adv Neural Inf Process Syst*. 2012:3032–3040.

Krishna BS, Semple MN. 2000. Auditory temporal processing: responses to sinusoidally amplitude-modulated tones in the inferior colliculus. *J Neurophysiol*. 84:255–273.

Langner G. 1983. Evidence for neuronal periodicity detection in the auditory system of the Guinea fowl: implications for pitch analysis in the time domain. *Exp Brain Res*. 52:333–355.

Langner G, Schreiner CE. 1988. Periodicity coding in the inferior colliculus of the cat. I. Neuronal mechanisms. *J Neurophysiol*. 60: 1799–1822.

Lee JH, Wang X, Bendor D. 2020. The role of adaptation in generating monotonic rate codes in auditory cortex. *PLoS Comput Biol*. 16:e1007627.

Li X, Nie K, Imennov NS, Won JH, Drennan WR, Rubinstein JT, Atlas LE. 2012. Improved perception of speech in noise and mandarin tones with acoustic simulations of harmonic coding for cochlear implants. *J Acoust Soc Am*. 132:3387–3398.

Lomber SG, Meredith MA, Kral A. 2010. Cross-modal plasticity in specific auditory cortices underlies visual compensations in the deaf. *Nat Neurosci*. 13:1421–1427.

Lomber SG, Meredith MA, Kral A. 2011. Adaptive crossmodal plasticity in deaf auditory cortex: areal and laminar contributions to supranormal vision in the deaf. *Prog Brain Res*. 191: 251–270.

Lomber SG, Payne BR, Cornwell P, Long KD. 1996. Perceptual and cognitive visual functions of parietal and temporal cortices in the cat. *Cereb Cortex*. 6:673–695.

Lomber SG, Payne BR, Horel JA. 1999. The cryoloop: an adaptable reversible cooling deactivation method for behavioral or electrophysiological assessment of neural function. *J Neurosci Methods*. 86:179–194.

Lu T, Liang L, Wang X. 2001a. Neural representations of temporally asymmetric stimuli in the auditory cortex of awake primates. *J Neurophysiol*. 85:2364–2380.

Lu T, Liang L, Wang X. 2001b. Temporal and rate representations of time-varying signals in the auditory cortex of awake primates. *Nat Neurosci*. 4:1131–1138.

Ma X, Suga N. 2001a. Corticofugal modulation of duration-tuned neurons in the midbrain auditory nucleus in bats. *Proc Natl Acad Sci U S A*. 98:14060–14065.

Ma X, Suga N. 2001b. Plasticity of bat's central auditory system evoked by focal electric stimulation of auditory and/or somatosensory cortices. *J Neurophysiol*. 85:1078–1087.

Malhotra S, Lomber SG. 2007. Sound localization during homotopic and heterotopic bilateral cooling deactivation of primary and nonprimary auditory cortical areas in the cat. *J Neurophysiol*. 97: 26–43.

Malmierca MS, Izquierdo MA, Cristaudo S, Hernandez O, Perez-Gonzalez D, Covey E, Oliver DL. 2008. A discontinuous tonotopic organization in the inferior colliculus of the rat. *J Neurosci*. 28: 4767–4776.

Markovitz CD, Tang TT, Lim HH. 2013. Tonotopic and localized pathways from primary auditory cortex to the central nucleus of the inferior colliculus. *Front Neural Circuits*. 7:77.

Mauk MD, Buonomano DV. 2004. The neural basis of temporal processing. *Annu Rev Neurosci*. 27:307–340.

Mioni G, Grondin S, Bardi L, Stablum F. 2020. Understanding time perception through non-invasive brain stimulation techniques: a review of studies. *Behav Brain Res*. 377:112232.

Moon IJ, Hong SH. 2014. What is temporal fine structure and why is it important? *Korean J Audiol*. 18:1–7.

Moore BC. 2012. Effects of bandwidth, compression speed, and gain at high frequencies on preferences for amplified music. *Trends Amplif*. 16:159–172.

Moser T. 2015. Optogenetic stimulation of the auditory pathway for research and future prosthetics. *Curr Opin Neurobiol*. 34:29–36.

Muller-Preuss P, Flachskamm C, Bieser A. 1994. Neural encoding of amplitude modulation within the auditory midbrain of squirrel monkeys. *Hear Res*. 80:197–208.

Neff WD, Casseday JH. 1977. Effects of unilateral ablation of auditory cortex on monaural cat's ability to localize sound. *J Neurophysiol*. 40:44–52.

Nelson PC, Smith ZM, Young ED. 2009. Wide-dynamic-range forward suppression in marmoset inferior colliculus neurons is generated centrally and accounts for perceptual masking. *J Neurosci*. 29: 2553–2562.

Nelson PC, Young ED. 2010. Neural correlates of context-dependent perceptual enhancement in the inferior colliculus. *J Neurosci*. 30: 6577–6587.

Newman JD, Kenkel WM, Aronoff EC, Bock NA, Zametkin MR, Silva AC. 2009. A combined histological and MRI brain atlas of the common marmoset monkey, *Callithrix jacchus*. *Brain Res Rev*. 62: 1–18.

Nourski KV, Brugge JF. 2011. Representation of temporal sound features in the human auditory cortex. *Rev Neurosci*. 22:187–203.

Nunez A, Malmierca E. 2007. Corticofugal modulation of sensory information. *Adv Anat Embryol Cell Biol*. 187:1–74 (1 p following table of contents).

Petkov CI, Bendor D. 2016. Neuronal mechanisms and transformations encoding time-varying signals. *Neuron*. 91:718–721.

Plakke B, Hwang J, Romanski LM. 2015. Inactivation of primate prefrontal cortex impairs auditory and audiovisual working memory. *J Neurosci*. 35:9666–9675.

Popelar J, Nwabueze-Ogbo FC, Syka J. 2003. Changes in neuronal activity of the inferior colliculus in rat after temporal inactivation of the auditory cortex. *Physiol Res*. 52:615–628.

Preuss A, Muller-Preuss P. 1990. Processing of amplitude modulated sounds in the medial geniculate body of squirrel monkeys. *Exp Brain Res*. 79:207–211.

Rees A, Moller AR. 1983. Responses of neurons in the inferior colliculus of the rat to AM and FM tones. *Hear Res*. 10:301–330.

Rees A, Moller AR. 1987. Stimulus properties influencing the responses of inferior colliculus neurons to amplitude-modulated sounds. *Hear Res*. 27:129–143.

Romo R, Salinas E. 2003. Flutter discrimination: neural codes, perception, memory and decision making. *Nat Rev Neurosci*. 4:203–218.

Rose GJ, Capranica RR. 1985. Sensitivity to amplitude modulated sounds in the anuran auditory nervous system. *J Neurophysiol*. 53: 446–465.

Rosen S. 1992. Temporal information in speech: acoustic, auditory and linguistic aspects. *Philos Trans R Soc Lond B Biol Sci*. 336:367–373.

Roth BL. 2016. DREADDs for neuroscientists. *Neuron*. 89:683–694.

Rouiller E, de Ribaupierre F. 1982. Neurons sensitive to narrow ranges of repetitive acoustic transients in the medial geniculate body of the cat. *Exp Brain Res*. 48:323–326.

Saldana E, Feliciano M, Mugnaini E. 1996. Distribution of descending projections from primary auditory neocortex to inferior colliculus mimics the topography of intracollicular projections. *J Comp Neurol*. 371:15–40.

Salinas E, Hernandez A, Zainos A, Romo R. 2000. Periodicity and firing rate as candidate neural codes for the frequency of vibrotactile stimuli. *J Neurosci*. 20:5503–5515.

Schuller G. 1979. Coding of small sinusoidal frequency and amplitude modulations in the inferior colliculus of 'CF-FM' bat, *Rhinolophus ferrumequinum*. *Exp Brain Res*. 34:117–132.

Singh NC, Theunissen FE. 2003. Modulation spectra of natural sounds and ethological theories of auditory processing. *J Acoust Soc Am*. 114:3394–3411.

Smith AL, Parsons CH, Lanyon RG, Bizley JK, Akerman CJ, Baker GE, Dempster AC, Thompson ID, King AJ. 2004. An investigation of the role of auditory cortex in sound localization using muscimol-releasing Elvax. *Eur J Neurosci*. 19:3059–3072.

Suga N. 2020. Plasticity of the adult auditory system based on corticocortical and corticofugal modulations. *Neurosci Biobehav Rev*. 113:461–478.

Suta D, Popelar J, Syka J. 2008. Coding of communication calls in the subcortical and cortical structures of the auditory system. *Physiol Res*. 57(Suppl 3):S149–S159.

Syka J, Popelar J, Kvasnak E, Astl J. 2000. Response properties of neurons in the central nucleus and external and dorsal cortices of the inferior colliculus in Guinea pig. *Exp Brain Res*. 133:254–266.

Theunissen FE, Elie JE. 2014. Neural processing of natural sounds. *Nat Rev Neurosci*. 15:355–366.

Vernier VG, Galambos R. 1957. Response of single medial geniculate units to repetitive click stimuli. *Am J Physiol*. 188:233–237.

Versteegh CP, Meenderink SW, van der Heijden M. 2011. Response characteristics in the apex of the gerbil cochlea studied through auditory nerve recordings. *J Assoc Res Otolaryngol*. 12:301–316.

Wang X. 2013. The harmonic organization of auditory cortex. *Front Syst Neurosci*. 7:114.

Wang X, Lu T, Bendor D, Bartlett E. 2008a. Neural coding of temporal information in auditory thalamus and cortex. *Neuroscience*. 154: 294–303.

Wang X, Lu T, Bendor D, Bartlett E. 2008b. Neural coding of temporal information in auditory thalamus and cortex. *Neuroscience*. 157: 484–493.

Warden MR, Cardin JA, Deisseroth K. 2014. Optical neural interfaces. *Annu Rev Biomed Eng*. 16:103–129.

Winer JA, Larue DT, Diehl JJ, Hefti BJ. 1998. Auditory cortical projections to the cat inferior colliculus. *J Comp Neurol*. 400:147–174.

Wood KC, Town SM, Atilgan H, Jones GP, Bizley JK. 2017. Acute inactivation of primary auditory cortex causes a sound localisation deficit in ferrets. *PLoS One*. 12:e0170264.

Xu K, Zhang J, Guo S, Zheng X. 2016. Optogenetic modulation of locomotor activity on free-behaving rats. *Methods Mol Biol*. 1408: 195–206.

Yan J, Ehret G. 2002. Corticofugal modulation of midbrain sound processing in the house mouse. *Eur J Neurosci*. 16:119–128.

Yao JP, Hou WS, Yin ZQ. 2012. Optogenetics: a novel optical manipulation tool for medical investigation. *Int J Ophthalmol*. 5: 517–522.

Zhang Y, Suga N, Yan J. 1997. Corticofugal modulation of frequency processing in bat auditory system. *Nature*. 387:900–903.

Zhou X, Jen PH. 2005. Corticofugal modulation of directional sensitivity in the midbrain of the big brown bat, *Eptesicus fuscus*. *Hear Res*. 203:201–215.

Zhou X, Jen PH. 2007. Corticofugal modulation of multi-parametric auditory selectivity in the midbrain of the big brown bat. *J Neurophysiol*. 98:2509–2516.